Polyamorphism in aluminate liquids

2003 J. Phys.: Condens. Matter 15 6105

(http://iopscience.iop.org/0953-8984/15/36/303)

INSTITUTE OF PHYSICS PUBLISHING JOURNAL OF PHYSICS: CONDENSED MATTER

J. Phys.: Condens. Matter **15** (2003) 6105–6121 PII: S0953-8984(03)65294-X

Polyamorphism in aluminate liquids

Paul F McMillan[1,2,4], Mark Wilson[1] and Martin C Wilding[3]

[1] Christopher Ingold Laboratory, Department of Chemistry, University College London, 20 Gordon Street, London WC1H 0AJ, UK
[2] Davy–Faraday Research Laboratory, Royal Institution of Great Britain, 21 Albemarle Street, London W1X 4BS, UK
[3] Department of Geology and McClellan Nuclear Radiation Center, University of California, Davis, CA 95616, USA

E-mail: p.f.mcmillan@ucl.ac.uk

Received 22 June 2003
Published 29 August 2003
Online at stacks.iop.org/JPhysCM/15/6105

Abstract

Supercooled liquids in the Y_2O_3–Al_2O_3 system undergo a liquid–liquid phase transition between a high-temperature, high-density amorphous polymorph (HDA form), and one with lower density that is stable at lower temperature (LDA form). The two amorphous polymorphs have the same chemical composition, but they differ in their density (∼4% density difference), and in their heat content (enthalpy) and entropy determined by calorimetry. Here we present new results of structural studies using neutron and high-energy x-ray diffraction to study the structural differences between high-density amorphous (HDA) and low-density amorphous (LDA) polyamorphs. The combined data sets show no large differences in the average nearest-neighbour Al–O or Y–O bond lengths or coordination numbers between the low- and high-density liquids. However, the data indicate that changes occur among the packing geometries and clustering of the Al–O and Y–O coordination polyhedra, i.e., within the second-nearest-neighbour shell defined by the metal–metal (i.e., Y–Y, Y–Al and Al–Al) interactions. Polarizable ion molecular dynamics simulations of Y_2O_3–Al_2O_3 liquids are used to help interpret the pair-correlation functions obtained from x-ray and neutron scattering data. Unexpectedly large density fluctuations are observed to occur during the simulation, that are interpreted as due to dynamic sampling of high- and low-density configurations within the single-phase liquid at temperatures above the critical point or phase transition line. Calculated partial radial distribution functions indicate that the primary differences between HDA and LDA configurations occur among the Y–Y correlations.

(Some figures in this article are in colour only in the electronic version)

[4] Author to whom any correspondence should be addressed.

1. Introduction

Recently, an unusual liquid–liquid phase transition phenomenon was reported among supercooled liquids in the Y_2O_3–Al_2O_3 system [1–4]. During hot-stage microscopy experiments that were originally designed to observe melting and recrystallization behaviour, a new low-temperature liquid phase was observed to nucleate and grow in the supercooled regime [1]. The liquid–liquid transformation process was arrested at the glass transition, so that samples of the high- and low-temperature liquids could be recovered as metastably coexisting glasses. Chemical analysis showed that the glasses had identical compositions, but back-scattered electron imaging studies indicated that they had different densities [1–5]. Calorimetry experiments using differential scanning and high-temperature solution techniques showed that the low-temperature (low-density; LDA form) and high-temperature, high-density (HDA form) glasses had different enthalpies and entropies [2, 6–8]. The purpose of the present study was to investigate the nature of the structural differences between the high-density amorphous (HDA) and low-density amorphous (LDA) polymorphs, using neutron and high-energy x-ray scattering techniques, combined with polarizable ion molecular dynamics (PIMD) simulations of the glassy and liquid phases.

The liquid–liquid phase transition observed to occur in the Y_2O_3–Al_2O_3 system at constant composition forms part of a newly described class of phenomena known generally as 'polyamorphism', that concerns the existence of distinct liquid phases or different amorphous states of a given substance as a function of the pressure and temperature, and the transformations between them [9–16]. The different liquid or glassy polymorphs or phases have different structures and thermodynamic properties, that occur at constant chemical composition. They are thus analogous to the different crystalline polymorphs of a given substance that appear as a function of P and T. The observation of polyamorphism and the underlying existence of density, entropy-driven liquid–liquid phase transitions is becoming recognized as a general occurrence among a wide range of chemical systems and bonding types, and it is being developed as a new phenomenology within the physical chemistry of liquids and glasses [12–16].

'Unmixing' events are observed between liquids or glasses with different limiting chemical compositions, and these form a well known process that occurs in response to gradients in the chemical potential. Liquid–liquid phase transitions that occur at constant composition instead represent a minimization of the free energy in response to the pressure (i.e., density differences between the amorphous polymorphs), or the temperature (entropy-driven transitions). In the case of stable or metastable (supercooled) liquids, the polyamorphic transitions constitute true thermodynamic transformations of the first order occurring between systems that are in internal thermal equilibrium. For polyamorphism occurring within glasses and other non-ergodic amorphous states, the transformations recorded as a function of the applied pressure or temperature appear as rapid changes in the structure or properties as a function of the P and T. For example, polyamorphism occurs in SiO_2 and GeO_2 glasses. At ambient pressure, the glass structures are dominated by tetrahedral SiO_4 and GeO_4 units. Applying high pressure causes formation of octahedrally coordinated SiO_6 and GeO_6 groups, as is found in high-pressure crystalline phases. In $V(P)$ plots of the relations, the glasses initially undergo a volume decrease analogous to the tetrahedrally coordinated crystals. Within a narrow pressure range, the volume drops rapidly to values approaching those of the high-density crystalline solids, with local structural configurations in high (predominantly sixfold) coordination [9, 15, 17–21]. Similar rapid changes in structure and properties as a function of the pressure have been recorded for amorphous Si and Ge [16, 22–24]. Such changes in the glassy or non-ergodic amorphous state might indicate the presence of an underlying liquid–liquid density-driven phase transition.

An early indication of the likelihood of liquid–liquid phase transitions occurring at constant composition arose from determinations of the melting relations of simple substances, as a function of the pressure (i.e., $\mathrm{d}T_\mathrm{m}/\mathrm{d}P$). Normally, it is expected that such slopes should be positive, because of the Clausius–Clapeyron relation:

$$\frac{\mathrm{d}T_\mathrm{m}}{\mathrm{d}P} = \frac{\Delta V_\mathrm{m}}{\Delta S_\mathrm{m}} = \frac{V_\mathrm{liquid} - V_\mathrm{crystal}}{S_\mathrm{liquid} - S_\mathrm{crystal}}. \tag{1}$$

The liquid is less ordered than the corresponding crystal, so that ΔS_m is always positive. The phenomenon of melting is also usually associated with an increase in volume (positive ΔV_m) because of increased thermal motion and the liquid accessing additional degrees of structural freedom. However, many simple systems show a *negative* melting slope, at least within certain pressure intervals, and there can be one or more maxima in the melting curves [13, 25–27]. Examples of elements exhibiting such behaviour include the metals Ba (melting curve maximum at 2 GPa; perhaps also two others between 6 and 8 GPa), Cs (a double maximum separated by the bcc–fcc phase transition at 2.5 GPa), Ti (negative initial slope to 8 GPa; likely maximum near 1 atm), Eu (maximum at 3 GPa) and Pu (negative initial slope to 3 GPa); the semiconductors Si and Ge (negative initial slopes, with potential maxima at 'negative pressures') and Se and Te (maxima at 5 and 2 GPa, respectively). Perhaps the best known compound with a negative initial melting slope is H_2O (ice Ih phase). Other materials also show melting curve maxima (KNO_2, KNO_3, Li_2CrO_4, Na_2SeO_4 and KH_2AsO_4), negative initial melting slopes (Li_2MoO_4 and the α-quartz form of GeO_2) or impending maxima intersected by triple points (e.g., the β-quartz and coesite forms of SiO_2) [28].

The existence of a negative melting slope implies that the liquid density has exceeded that of the underlying crystalline phase. In a single-component system, this is most readily and intuitively understood in terms of a liquid model that contains low- and high-density structural 'species', that are present in variable amounts as a function of the pressure. This is termed a 'two-state', or 'two-domain', model of the liquid. The low-density species could correspond to domains of the liquid structure containing configurations like those present in low-density crystalline phases, and the high-density species could be related to structures encountered in higher-density crystals. In the crystalline state, all local coordination environments must transform at the same transition pressure. However, the disordered liquid state permits the coexistence of low- and high-density domains in the liquid, with relative proportions that can change continuously with increasing pressure. There is thus an additional component to the liquid compressibility, due to the increased proportion of high-density domains, and at some pressure the liquid density will exceed that of the corresponding crystal.

To achieve a thermodynamic description of such a two-state liquid, Rapoport [29, 30] first applied Guggenheim's mixing model [31], now known as the 'regular solution' thermodynamic model, to the liquid phase in order to calculate the melting relations. He thus assumed that there would be some enthalpic 'signature' associated with mixing the two liquid states or species, with their different structures and contributions to the density. To aid in intuitive interpretation, the mixing energy can be thought of as arising directly from specific interactions between the low- and high-density domains, if these are considered to represent actual structural species in the liquid, or it can be accepted more generally as a contribution to the free energy of the liquid arising from the cooperative bonding rearrangements that must occur during mixing of two distinct structural species or domains within the dynamic liquid structure. The low- and high-density species were treated by Rapoport as thermodynamic components (A and B), and their relative proportions described as mole fractions (X_A, X_B), in calculating the free energy relations of the two-state liquid.

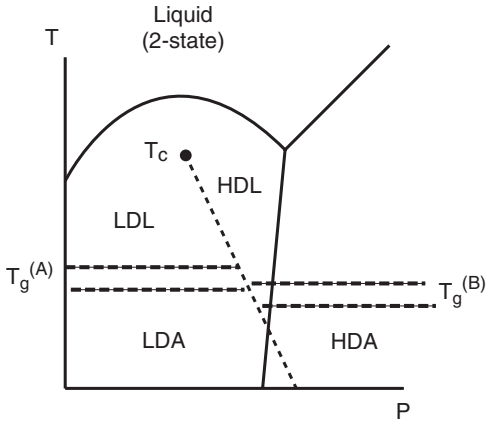

Figure 1. Schematic diagram illustrating the relationship between the existence of a melting curve maximum, requiring the establishment of a two-state model to describe the liquid density and thermodynamic properties, and the development of a critical point (T_c) and line of first-order density-driven liquid–liquid phase transitions, according to the model of Rapoport [29, 30]. Because the amplitude of the two-state mixing parameter (W) is generally expected to be smaller than the latent heat of fusion (ΔH_m), the critical point is expected to lie below the melting curve, in the metastable supercooled liquid state regime. This 'rule of thumb' may be bypassed in certain cases, such as that of liquid phosphorus [39, 40]. Above their respective glass transitions ($T_g^{(A)}$, $T_g^{(B)}$), the HDA and LDA phases are in their internally equilibrated liquid forms (HDL, LDL). As the T is decreased, they encounter their respective glass transitions, and become the non-ergodic HDA and LDA glassy forms.

The application of the two-state model transformed the consideration of a one-component system in P–T space into a problem with an effective additional 'compositional' variable (or 'axis', in a P–T–X_A plot [15]), corresponding to the relative proportions of high- and low-density species present. Although these species have the same chemical composition: they are distinguished by their different local structures and partial thermodynamic quantities $\bar{V}$, $\bar{H}$, $\bar{S}$ etc. One characteristic property of any regular solution mixing model is the appearance of a critical point in the free energy–'composition' relations (i.e., $\mu - X_A$) as the temperature is reduced below a critical value (T_c). The value of T_c is determined by the magnitude, or 'strength', of the thermodynamic mixing parameter W, expressed in kJ mol^{-1}. Above T_c, the liquid consists of a single phase containing an equilibrium distribution of low- and high-density species or domains: this is the one-phase regime for the two-state liquid. Below T_c, the free energy function develops a double minimum as a function of X_A or X_A, that strengthens as the temperature is lowered [15, 29]. This indicates the presence of distinct liquid phases (i.e., low-density liquid (LDL) and high-density liquid (HDL)), with characteristic relative proportions of the LDL and HDL components, that are separated by a first-order phase transition [1, 2, 10–16, 29]. As the pressure is varied, so also is the temperature of the LDL–HDL liquid–liquid transition ($T_{L–L}$), depending upon the volume and enthalpy contrast between the low- and high-density components. The result is a line of first-order liquid–liquid phase transitions extending in P–T space, with a Clapeyron slope ($dT_{L–L}/dP$) that could be negative or positive (although various arguments and experimental observations to date indicate that $dT_{L–L}/dP$ slopes might generally have negative values [15]) (figure 1). Although his model had indicated the thermodynamic basis for the potential occurrence of such density-, entropy-driven liquid phase transitions at constant composition, and Rapoport [29, 30] noted this fact, he did not pursue the argument further.

In a review of the phenomena associated with 'pressure induced amorphization', Ponyatovsky and Barkalov [16] later extended the analysis to include discussion of the two-phase region below T_c, using data from 'corresponding crystals' to estimate partial thermodynamic quantities for the low- and high-density liquid species, using Si and Ge as examples. They identified both the line of first-order LDL–HDL phase transitions, and the associated spinodals to low and high density. Recent experimental results and computer simulations have now confirmed those predictions [24, 32–35].

Based on general considerations for the thermodynamics it is expected that L–L transitions will occur below the liquidus, in the supercooled liquid regime [10, 15]. Typical values of the interaction parameter W range from 10 to 30 kJ mol^{-1} [6, 7, 16, 24]. This is generally much smaller than the enthalpy change associated with melting, so that the calculated critical temperature lies below the melting point. This means that passage from the single-phase, two-state liquid into the two-phase regime containing the LDL–HDL transition would generally occur in the metastable supercooled liquid regime, below the melting point. This observation has consequences for the observation and study of the L–L transition, that must compete with crystallization kinetics in the highly metastable regime [10]. The glass transition may also intervene, for one or both of the LDL or HDL phases (i.e., T_g^A, T_g^B), resulting in the non-ergodic solid amorphous materials, LDA and HDA.

Brazhkin and others have long suggested the occurrence of phase transitions in elemental liquids such as Se, S, Te, I and P, based on observations of abrupt changes in the electrical conductivity observed with increasing density, analogous to those associated with insulator/semiconductor–metal transitions in crystalline solids [11, 16]. The group has recently described the physical property changes occurring in the stable liquid regime in terms of 'quasi-phase transitions' extending into the liquid phase, among fluctuating nano- to micro-sized domains of LDA and HDA 'phases'. The question of the effects of domain size upon the thermodynamic properties of mixed systems is currently being re-examined, as the domains enter the nanoscale size regime [36–38]. In the case of liquid phosphorus, a recent study based on x-ray scattering and tomography described a liquid–liquid transition between HDA (monomeric) and LDA (polymeric) phases extending into the stable liquid regime, thus indicating the presence of a crystal–L_1–L_2 triple point at ∼1 GPa and ∼1000 K [39]. The density jump at the L–L transition is 40%, an unexpectedly large value [40]. A recent study has now indicated that the transition occurring at high temperature above the liquidus is in fact a transition between the high-density liquid L_2, and the low-density L_1 phase in its supercritical fluid state; i.e., L_1 is above its one-phase critical point, and the true density-driven liquid–liquid phase transition probably occurs at much lower temperature, below the liquidus [41].

Direct visual evidence for the occurrence of a density-driven phase transition between two liquids in the supercooled regime was first observed in the system Y_2O_3–Al_2O_3 [1, 2]. This is an unusual example of a system that is chemically multi-component in nature, and that *could* unmix in response to compositional fluctuations. However, it does not appear to do so. Here, we summarize those observations, along with results of our recent experimental and simulation studies of the system to determine the structural nature of the differences between the HDA and LDA configurations.

2. Y_2O_3–Al_2O_3 liquids

Liquids in the system Y_2O_3–Al_2O_3 give rise to important ceramic materials, including the laser host crystal 'YAG' (i.e., $Y_3Al_5O_{12}$ garnet) [41–45]. The phase relations near the YAG melting point and also the metastable phase behaviour in the system have been investigated intensively, and the results indicate several unusual features [41–48]. Growth of YAG single crystals for

technological applications is achieved by a Czochralski process following melting of sol–gel derived precursors. Melting and recrystallization have also recently been investigated in the absence of a crystalline substrate. It was found that, if the temperature did not exceed 30–40 °C above the liquidus, growth of microcrystalline YAG particles was observed to occur upon cooling [41–43]. However, if the melt were taken to higher temperatures, crystallization of the garnet phase was bypassed during cooling, and metastable mixtures of Al_2O_3 corundum (C) and $YAlO_3$ perovskite (YAP) resulted instead. Those observations gave rise to speculations that some type of structural ordering, or perhaps even a structural 'transition', might occur within the high-temperature liquid [41]. It is now known that the origin of the observed phase behaviour is kinetic in nature. Crystallization and melting of YAG is sluggish, and crystalline nuclei present from the sol–gel synthesis persist above liquidus temperatures for normal heating durations: these crystallites can then provide nucleation sites for YAG growth upon cooling. However, once such nuclei are eliminated by heating to higher temperatures or for longer times, the metastable phase mixture (i.e., corundum + YAP) nucleates and grows rapidly during cooling at the expense of the garnet phase. The possible occurrence of liquid–liquid phase separation within high-temperature Y_2O_3–Al_2O_3 liquids had in fact been suggested in early studies, based upon the appearance of opalescence in the liquid [48]. However, similar opalescence also occurs for the end-member liquid Al_2O_3, and this is now thought to be due to light scattering occurring as a result of density fluctuations within the rapidly convecting samples, that have very low viscosity.

The true L–L transition that occurs within supercooled liquids in the Y_2O_3–Al_2O_3 system was observed to occur over a wide range of compositions: it was concluded that the dominant thermodynamic parameters driving the transition were the density and entropy differences between low- (LDL) and high- (HDL) density supercooled liquid phases [1–8]. The transition was observed to occur below the equilibrium solidus during rapid cooling of liquids with bulk compositions between 24 and 32 mol% Y_2O_3 [1]. The L–L phase transition resulted in separation of a second liquid phase as 'droplets' within a 'matrix' of the high-temperature liquid, before both were quenched to metastably coexisting glasses [1–8]. The compositions of 'droplet' and 'matrix' were determined by electron microprobe analysis to be identical, for the entire suite of samples with different *bulk* compositions. In the original study, the relative densities of the two glasses were inferred from contrast measurements in back-scattered scanning electron microscopy images obtained along with the electron microprobe analyses [1, 3]. Because it formed high-brightness areas, the 'matrix' glass that was derived from the high-temperature liquid phase was determined to be the HDA form. The lower-density amorphous (LDA) phase that formed near-spherical inclusions was derived from the liquid that nucleated and grew at lower temperatures during the quench in the Ir-wire studies. The HDA and LDA glassy forms are readily identified and distinguished by (a) their mechanical properties (the LDA form is harder than the HDA glass, so it develops greater relief and shows fewer scratches than the HDA phase upon polishing), and (b) calorimetry: the HDA form has a lower T_g (onset 830–840 °C) than the LDA phase (∼1020–1030 °C) [2, 4, 6–8], so that the two can be distinguished by determinations of their structural relaxation, including direct observation *via* hot-stage microscopy.

Recent experiments have confirmed the occurrence of an HDA–LDA transition in the Y_2O_3–Al_2O_3 system. Thermodynamic measurements on HDA and LDA glassy samples by differential scanning calorimetry (DSC) and solution calorimetric techniques have revealed differences in the heat content and entropy between the LDA and HDA liquid and glassy phases [2, 6, 7], and preliminary neutron scattering measurements have revealed differences in the Y/Al packing and Al–O–Y connectivity schemes that distinguish the two liquid structures [8]. A key thermodynamic quantity that remained to be measured was a direct

determination of the densities of coexisting HDA and LDA glasses in the Y_2O_3–Al_2O_3 system. Previously, it was not possible to physically separate/isolate the tiny samples available from 'wire-loop' heating experiments, for macroscopic density measurements. We have since prepared suitable samples of HDA–LDA Y_2O_3–Al_2O_3 samples *via* roller-quenching techniques. These preparations resulted in a few samples that contained sufficient coexisting 'matrix' and 'inclusion' glassy phases, that could be physically separated to carry out absolute density determinations by sink–float techniques. Density measurements on glassy 'matrix' and 'inclusion' samples on one sample containing 24 mol% Y_2O_3 (AY-24) were carried out using mixtures of deionized water ($\rho = 1.00$ g cm^{-3}) and thallium malonate–formate solution (i.e., Clerici's solution, $\rho = 4.36$ g cm^{-3}) as the suspending liquid. Aliquots of Clerici's solution were added to a tube containing the sample and a known amount of water, using ultrasonic treatments to homogenize the solution [49]. Density measurements were made by direct optical examination of the degree of sinking or flotation of the glass samples, compared with appropriate density standards including fragments of Al_2O_3 (3.965 g cm^{-3}) and MgO (3.58 g cm^{-3}). Experiments were carried out with glass fragments and standards both separately and together, in various combinations, to determine relative and absolute densities. For more precise observations, the samples were side illuminated by monochromatic light from a He–Ne laser during the sink–float measurements. The results showed that the HDA glassy phase was 4% more dense than the LDA polyamorph (3.72 ± 0.01 and 3.58 ± 0.01 g cm^{-3}, respectively). Both values are considerably lower than the densities of crystalline YAG (4.55 g cm^{-3}), or the metastable garnet-structured solid solution at the AY-24 composition (4.00 g cm^{-3}).

3. Neutron and x-ray diffraction studies of Y_2O_3–Al_2O_3 glasses

The differences recorded in the density and entropy between the LDA and HDA phases of Y_2O_3–Al_2O_3 at fixed composition imply structural differences between the two polyamorphs, that should be observable by x-ray and neutron scattering. Neutron and x-ray diffraction data have been collected for two yttrium-aluminate glass samples to investigate the changes in structure that occur associated with the HDL–LDL transition. One sample studied (AY-25) was a single-phase HDA glass, quenched metastably from the stable HDL liquid, bypassing the HDL–LDL transition during the quench [2, 8]. The other sample (AY-20) is a two-phase glass containing both HDA and LDA polyamorphs in metastable co-existence, due to partial sampling of the HDL–LDL transition during quenching. Details of the sample preparation and characterization, and the neutron and x-ray scattering experiments, are described elsewhere [2, 4, 6–8].

The neutron data provide an important constraint on the nearest-neighbour coordination number around both Al^{3+} and Y^{3+} ions. The mean Al–O coordination number is 4.16 and 4.28 for the single- and two-phase glass samples based on evaluation of the integral between minima in the total pair-correlation function [18]. The Al–O peak is observed in both AY-25 and AY-20 radial distribution functions at 1.8 Å, confirming a dominantly fourfold coordination environment for Al–O (figure 2). ^{27}Al NMR studies indicate that five- and sixfold coordinated Al environments are also present [4, 50]. There is no observable change in peak position, intensity or width of the Al–O correlation function between the HDA and LDA phases, indicating that the Al^{3+} first-neighbour environments remain unchanged across the transition.

The Y–O coordination number is 6.68 for the single-phase, HDA, glass. This value is smaller than for the crystalline solids $Y_3Al_5O_{12}$ and $YAlO_3$, so that there is a reduction in Y–O coordination on melting and subsequent quenching to glass. When the radial distribution functions for the two glasses are compared there are differences in the distance range 2–4 Å that

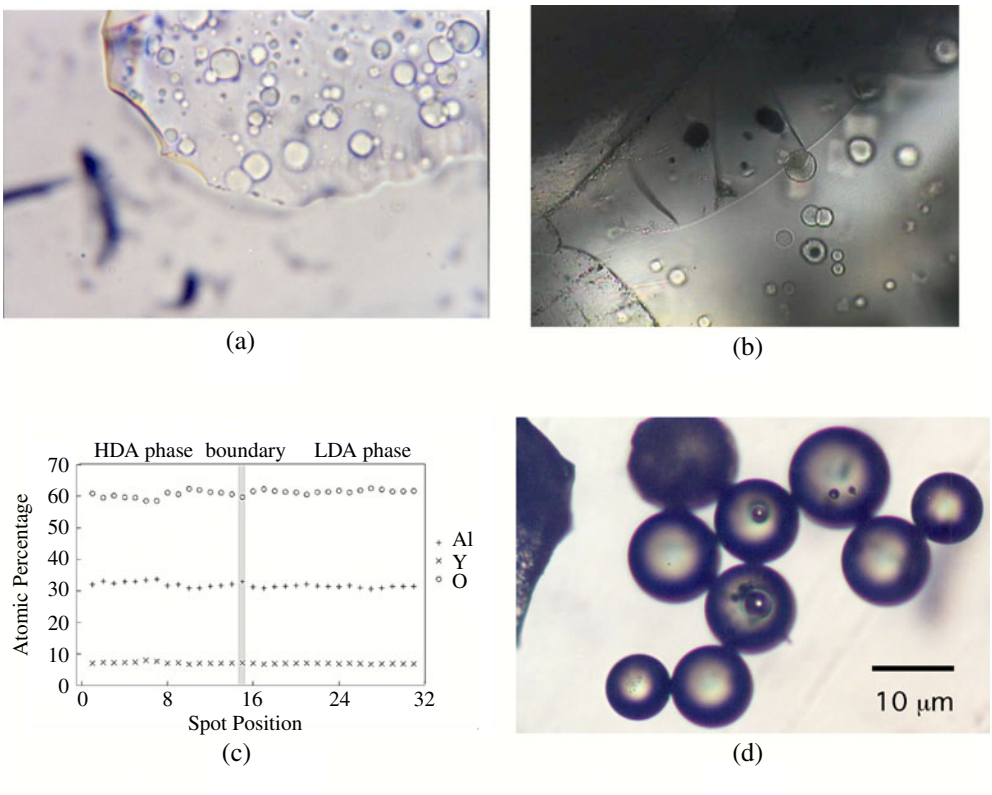

Figure 2. Metastably co-existing HDA and LDA regions within Y_2O_3–Al_2O_3 glass samples as a result of the polyamorphic HDL–LDL phase transition. (a) A thin edge of a sample prepared by roller quenching techniques: the LDL phase has started to nucleate and grow as sub-spherical inclusions within the 'matrix' of HDL phase (that corresponds to the stable liquid at high temperature), before being arrested by the glass transition during the quench. (b) An interface between HDA (bottom right) and LDA (top left to middle) phases in a sample prepared by Xe image heating and drop quenching. The LDA phase is tougher and is more resistant to polishing, as well as being less dense than the HDL phase (the density contrast is ∼4%). (c) Electron microprobe traverse (analysis for Al, Y and O) across the HDA–LDA interface in samples such as (a) and (b). (d) In one case, it was possible to physically separate macroscopic amounts of HDA and LDA phases for independent bulk density determination.

suggest, at first sight, additional Y–O correlations in the partly transformed glass. There are additional peaks superimposed on the O–O correlation, centred at 2.8 Å. Initially, we had thought that this might be due to a more regular Y–O coordination environment in the LDL glass [8]. However, this interpretation is not supported by ^{89}Y NMR spectra, that suggest little or no changes in the Y–O environment between the two polyamorphs [4, 6, 50].

High-energy x-ray diffraction studies are used to provide diffraction data that are complementary to the neutron scattering data. The neutron scattering data are dominated by pair correlation contributions involving oxygen. This means that changes in the medium-range order, associated with the metal–metal interactions in the second coordination shell at 3–5 Å, are masked by the O–O correlations (figure 2). With high-energy x-rays, which are able to penetrate deeply into the glass samples and act as a probe of the bulk glass structure, diffraction data can be obtained to values of scattering vector as high as 20 Å^{-1}. Fourier transformation of these data provides radial distribution functions giving information on the

Y–Y, Y–Al and Al–Al distances in the two glass samples, with minimal O–O contributions. Taking weighted difference functions between the two (i.e., neutron versus x-ray) $S(Q)$ data sets can be used to eliminate certain contributions to the structure factor. In figure 2(b), we show the radial distribution functions with the O–O contribution removed.

In the pair-correlation function derived from the difference $S(Q)$, the main differences between the HDA and LDA glass structures become more apparent. The Y–O distances and their asymmetric distribution, with a tail in the Y–O correlation to higher values of radial distance, are the same for each polyamorph. Both samples contain distorted Y–O polyhedra with between six and seven nearest-neighbour oxygens surrounding the yttrium ion. In the two-phase glass, the Y–O polyhedron may be slightly more regular, as evidenced by additional Y–O correlations present at smaller r, but the main differences between the samples appear as an increase in the intensity of the peak at 3.1 Å for the (HDA + LDA) sample compared to the single-phase (HDA) glass. The single-phase (HDA) glass has a prominent peak at 3.5 Å, resulting from overlapping Y–Y, Y–Al and Al–Al correlations, which reflect different configurations of the Al–O and Y–O polyhedra. In the two-phase sample, this peak has shifted to a lower value, and an additional feature has appeared at between 4 and 5 Å. These data suggest that the configurations defined by linking the polyhedral structural units are quite different in the two glasses. We have begun to carry out reverse Monte Carlo simulations based on the neutron and x-ray data to begin to gain a structural picture of the two glassy polymorphs [6]. For the HDA form, the Y–O polyhedra are predominantly edge shared with other YO_6/YO_7 units (figure 3). The growth of the peak at 4.5 Å following the HDA–LDA transition indicates an increased proportion of corner-shared YO_n polyhedra. The Y–O units are mostly corner shared with AlO_4 polyhedra in the HDA phase, consistent with increased disorder and higher configurational entropy. Upon transition, a greater proportion of the Y–O and Al–O units become linked by edge sharing (figure 4).

4. Molecular dynamics studies of Y_2O_3–Al_2O_3 liquids

The results of diffraction studies offer valuable insights into the local ion–ion structural arrangements present in the Y_2O_3–Al_2O_3 glasses and the liquids they are derived from, and permit us to begin to probe the energetic driving forces behind the density, entropy-driven liquid–liquid phase transition. However, despite the complementary x-ray and neutron scattering experiments carried out on the same samples, there is still no clear atomic-level picture of the structural differences between the LDA and HDA phases. We have now extended the study by carrying out polarizable ion molecular dynamics studies of Y_2O_3–Al_2O_3 liquids, and have used the resulting simulated total scattering and pair correlation functions to interpret the x-ray and neutron data and begin to understand the structural nature of the HDL–LDL transition.

The potential models used here are relatively simple (and hence computationally tractable) pair-potential based ionic models (in which the ions carry their full formal valence charges) augmented with a description of the (many-body) ion polarization (termed a polarizable-ion model—see [51] for a review and calculation details). The parameters which control these models are derived from well directed electronic structure calculations [52].

Molecular dynamics simulations were performed on systems containing 640 ions at the 20 mol% (AY-20) and 25 mol% (AY-25) Y_2O_3 compositions. The choice of cell size offers a reasonable compromise between accessible length- and timescales. Constant pressure and temperature (NPT ensemble) are maintained throughout by using Nosé–Hoover thermostats [53] and isotropic barostats [54]. Models of this type have been shown to reproduce the liquid diffraction patterns of a range of molten oxides, for example, Al_2O_3 [23].

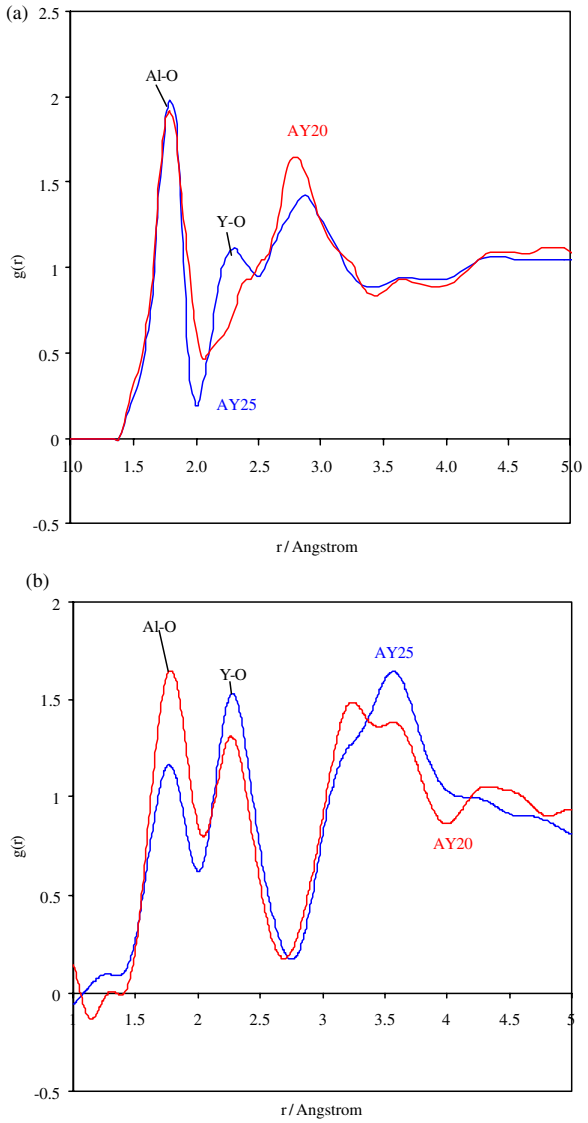

Figure 3. (a) Neutron pair correlation function for single-phase (AY-25: HDA) and two-phase (AY-20: HDA + LDA) yttrium-aluminate glass. This radial distribution function is obtained by minimum-noise Fourier transform of the total structure factors collected to a maximum value of scattering vector of 40 $Å^{-1}$. The first peak at 1.8 Å is the Al–O correlation and indicates a dominantly fourfold coordination environment around Al^{3+} ions. The peak at 2.3 Å in the AY-25 glass is the Y–O correlation. In the AY-20 glass the Y–O correlation has changed, with contributions at lower r and apparently at higher r, superimposed on the main O–O peak at 2.8 Å. (b) Pair correlation function for the same two glass samples produced from a difference plot ($\Delta S(Q)$) resulting from combined neutron and x-ray diffraction data. In this plot the contribution of O–O to the pair correlation function is eliminated. Differences in the Al–O and Y–O peaks reflect the compositional differences between the AY-25 and AY-20 glass, and no additional Y–O correlations are apparent in this difference plot. However, a large difference between the two glass structures is seen in the metal–metal correlations between 3.5 and 5 Å. In the AY-20 sample the peak at 3.1 Å becomes more prominent (the Y–Al contribution) while the peak at 4.5 Å (Y–Y) increases in intensity. This is interpreted as due to changes in the connectivity of Y–O and Al–O coordination polyhedra.

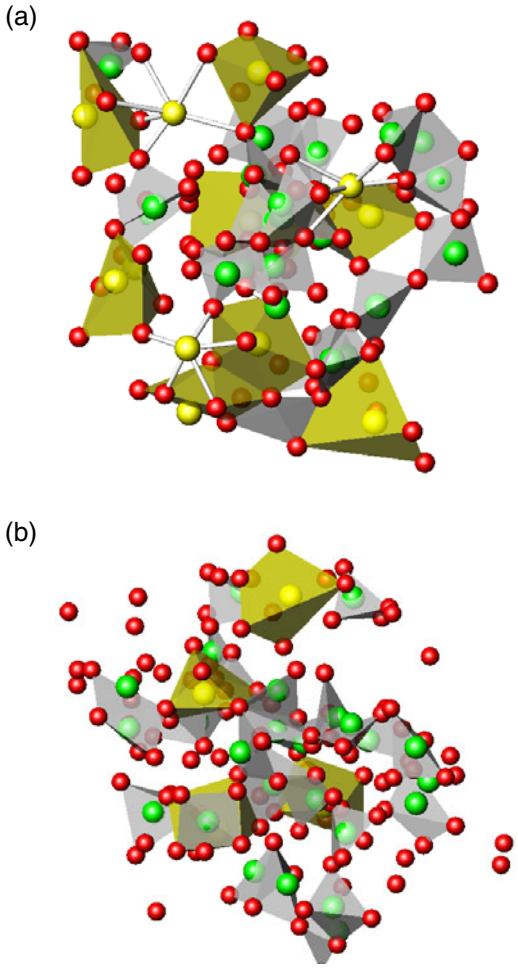

Figure 4. Results of a reverse Monte Carlo simulation of relative atomic positions and polyhedral arrangements in (a) AY-25 single-phase HDA and (b) AY-20 HDA + LDA samples, from neutron scattering data [8].

The partial structure factors are calculated directly from the Fourier components of the individual ion sub-densities, $S_{\alpha\beta}(k) = \langle A^*_\alpha(k) \cdot A_\beta(k)\rangle$, with $A_\alpha(k) = \sum_{i=1}^{N\alpha} \exp(\mathrm{i}k \cdot r_i)$. The three-component systems considered here give a total of six partial structure factors. In order to construct the total structure factors, $F(k)$, weighted sums of these partial structure factors must be generated. For the total neutron scattering function, $F^{\mathrm{nd}}(k)$, this sum is given by

$$F^{\mathrm{nd}}(k) = b_{\mathrm{O}}^2 c_{\mathrm{O}}[S_{\mathrm{OO}}(k) - 1] + 2b_{\mathrm{Al}}b_{\mathrm{O}}\sqrt{c_{\mathrm{Al}}c_{\mathrm{O}}}S_{\mathrm{AlO}}(k) + 2b_{\mathrm{Y}}b_{\mathrm{O}}\sqrt{c_{\mathrm{Y}}c_{\mathrm{O}}}S_{\mathrm{YO}}(k) + b_{\mathrm{Al}}^2 c_{\mathrm{Al}}[S_{\mathrm{AlAl}}(k) - 1] + b_{\mathrm{Y}}^2 c_{\mathrm{Y}}[S_{\mathrm{YY}}(k) - 1] + 2b_{\mathrm{Y}}b_{\mathrm{Al}}\sqrt{c_{\mathrm{Al}}c_{\mathrm{Y}}}S_{\mathrm{AlY}}(k) \qquad (2)$$

where c_α is the mole fraction of component α and b_α is the corresponding coherent neutron scattering length. In order to calculate the total x-ray scattering function, $F^{\mathrm{xrd}}(k)$, the scattering lengths in this equation must be replaced by the (k-dependent) x-ray form factors.

Figure 5 shows the calculated x-ray and neutron total scattering function for the AY-20 composition generated at a constant temperature of 2400 K over 2.2 ns of ion dynamics. Both functions are in excellent agreement with experiment, with the neutron scattering function

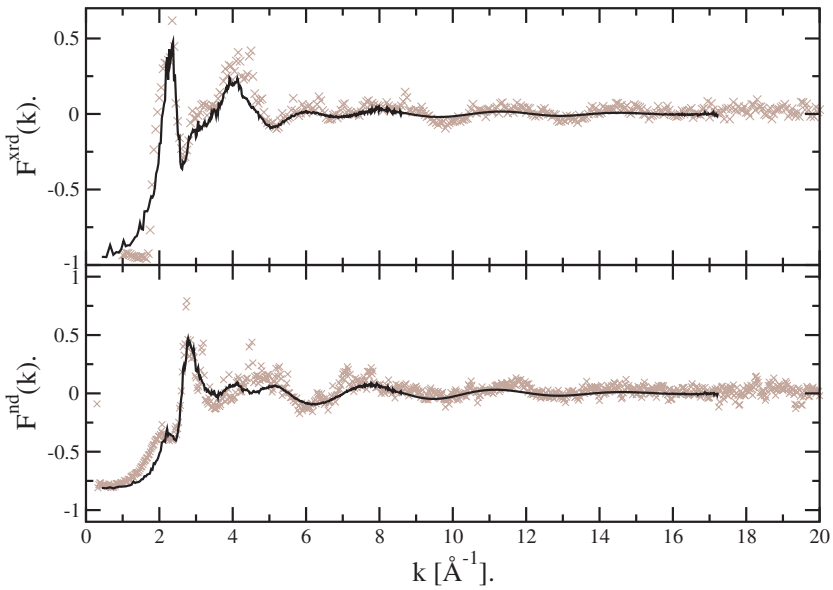

Figure 5. Calculated x-ray (upper panel) and neutron (lower panel) total scattering function for the AY20 composition generated at a constant temperature of 2400 K over 2.2 ns of ion dynamics. In both cases the simulated functions (solid curves) are compared with the experimental data (crosses).

showing only some small discrepancies with respect to experiment beyond the major peak (at $\approx$2.6 Å^{-1}). It is clear from the figure that the two total scattering functions have very different topologies. The strong peak at 2.3 Å^{-1} in $F^{\mathrm{xrd}}(k)$ appears only as a weak shoulder in $F^{\mathrm{nd}}(k)$. Furthermore, the strong main peak in $F^{\mathrm{xrd}}(k)$ (at 4.0 Å^{-1}) has only a very low-intensity corresponding feature in $F^{\mathrm{nd}}(k)$. In addition, the high-k oscillations have subtly different wavelengths.

Figure 6 shows the breakdown of the total x-ray and neutron scattering functions into the weighted contributions from the six partial structure factors. The x-ray scattering function is dominated by the Y–Y pair contribution, $S_{\mathrm{YY}}(k)$. Although the mole fraction of the yttrium sub-density is relatively small, the greater number of electrons in this ion with respect to either the aluminium or oxide ions (which are isoelectronic) leads to a much larger form factor weighting for the partial structure factors which include yttrium. The other partial structure factors play a significant role in determining the peak positions and shapes over different scattering angle ranges in $F^{\mathrm{xrd}}(k)$. The main peak is shifted to slightly higher k with respect to that in $S_{\mathrm{YY}}(k)$ by significant contributions from $S_{\mathrm{AlY}}(k)$, $S_{\mathrm{OO}}(k)$ and $S_{\mathrm{AlAl}}(k)$. In addition, the oscillation at larger scattering angles ($\geqslant$5 Å^{-1}), which we anticipate as being important in terms of defining the nearest-neighbour ion–ion separations and coordination environments, appears to be less dominated by $S_{\mathrm{YY}}(k)$ (which becomes relatively featureless at larger scattering angles) and more the result of strong oscillations in $S_{\mathrm{AlY}}(k)$, $S_{\mathrm{AlO}}(k)$, $S_{\mathrm{YO}}(k)$ and $S_{\mathrm{AlAl}}(k)$.

For the total neutron scattering function the similarity of the scattering lengths for the three ions means that the relative weightings of the six partial structure factors are dominated by the mole fraction of each ion type and, as a result, are largely dominated by $S_{\mathrm{OO}}(k)$. Again, however, the other functions play a crucial role in determining the precise position and shape of the peaks. The main peak in $F^{\mathrm{nd}}(k)$ is shifted to larger scattering angle with respect to that in $S_{\mathrm{OO}}(k)$ via strong contributions from $S_{\mathrm{AlO}}(k)$ and $S_{\mathrm{YO}}(k)$. The 'shoulder' on the main

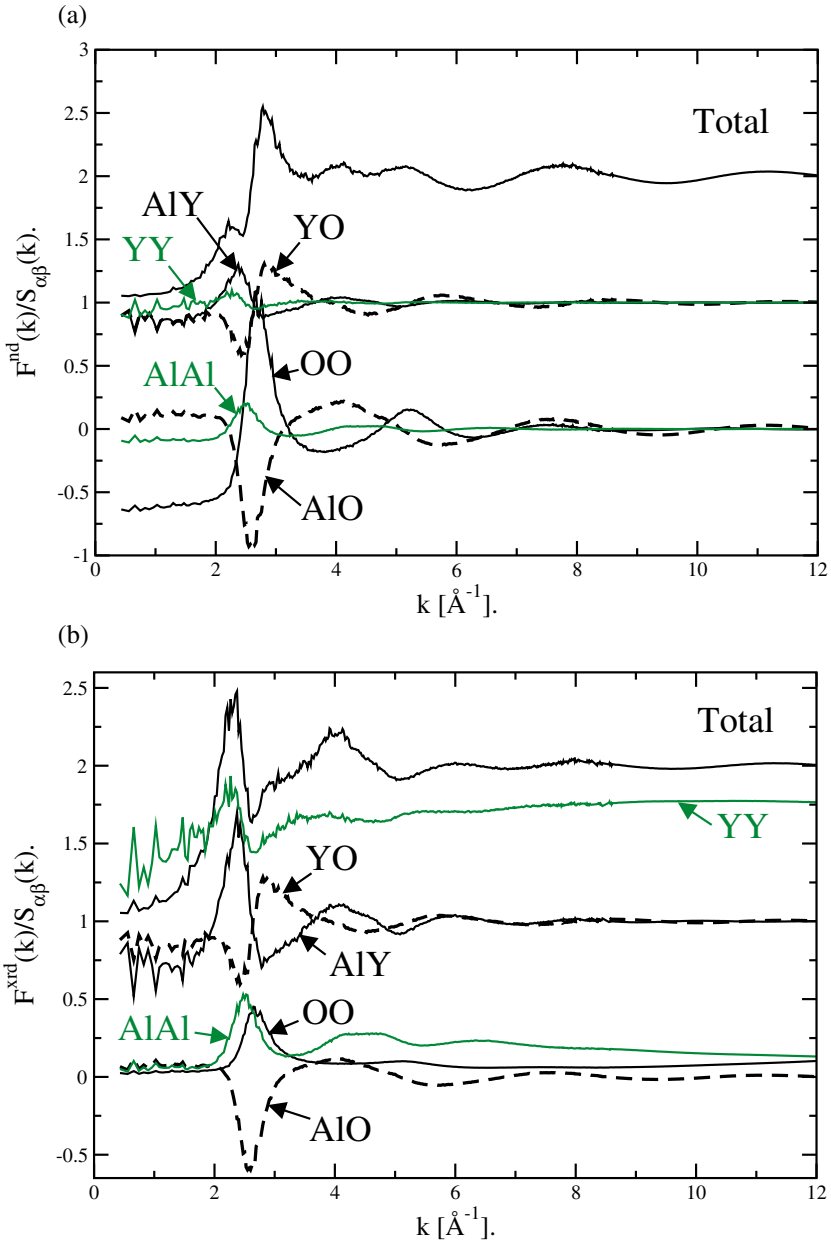

Figure 6. (a) Calculated partial structure factors for total neutron scattering function for AY-20 liquid at 2400 K. The individual partial structure factors are weighted according to equation (2). The Y–Y, Al–Y and Y–O curves have been shifted along the y-axis for clarity. The upper (black) curve is the total scattering function obtained by summing the individual partial structure factors. This has also been shifted along the y-axis for clarity. (b) Calculated partial structure factors for total x-ray scattering function for AY-20 liquid at 2400 K. The partial structure factors are shown weighted by the appropriate form factors and are shifted along the y-axis, as above.

peak at 2.2 Å^{-1} appears to result from contributions from $S_{\mathrm{AlY}}(k)$ and $S_{\mathrm{YY}}(k)$. The region at scattering angles immediately beyond the main peak shows poorest agreement with experiment.

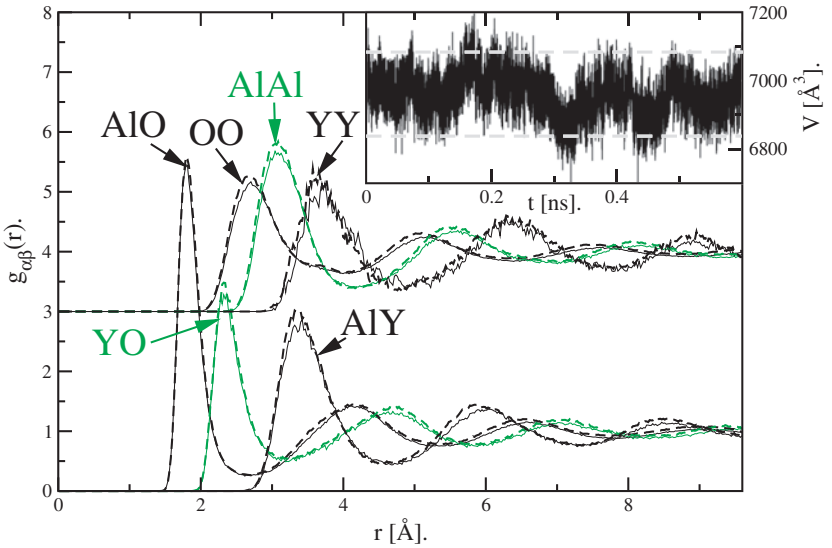

Figure 7. Calculated partial radial distribution functions for AY-20 liquid at 2400 K. The inset shows the fluctuation of the whole cell volume for a short (0.6 ns) section of the whole dynamics simulation at this temperature. The light dashed curves in the inset show the locations of the volumes two standard deviations away from the mean volume. The major body of the figure shows the partial rdfs calculated above and below these limits. The high-density limit curves are shown as dashed curves and the low-density limit curves as solid lines. The O–O, Al–Al and Y–Y prdfs have been shifted along the *y*-axis for clarity.

In this region there is near-perfect cancellation of the contributions from the different partial structure factors. As a result, slight imperfections in the model or the combination of the partials are magnified as a relatively large discrepancy in $F^{\mathrm{nd}}(k)$.

The figures shown above indicate that these relatively simple simulation models do reproduce both the experimental neutron and x-ray total structure factors. Given this, performing constant-pressure molecular dynamics allows us to monitor the system density as a function of time. For a simple ionic system, such as NaCl, the density would be expected to simply oscillate about the mean as a result of instantaneous pressure fluctuations inherent in the small cells. In the present case, however, the density is found to fluctuate significantly over the course of the whole run (see the inset to figure 7) remaining at high and low densities for considerable periods of time. Such behaviour indicates that the system is sampling characteristic high- and low-density configurations within the liquid, that might correspond to those that define the HDL and LDL polyamorphs. The simulations are performed significantly above the melting point in order to allow the ions to effectively sample phase space on typical simulation timescales. Because the melting point lies at higher temperature than the HDL–LDL phase transition and critical point, the state point under investigation is in the single-phase regime. However, within this regime, the system can still sample configurations with local ion geometries consistent with the high- and low-density two-phase region; the system energy is simply much greater than the barrier that must separate the HDA and LDA configurational 'basins'.

The possible atomistic origin of the structural differences responsible for these relatively large volume fluctuations can be understood by reference to the partial radial distribution functions (prdfs). Figure 7 shows the partial radial distribution functions calculated from

configurations coloured by reference to the system density. In this case only configurations less than or greater than two standard deviations away from the mean density are used to calculate the pair functions. The location of these limits is indicated in the inset to the figure. The metal–oxygen prdfs show only slight differences in the high- and low-density limits, indicating that the cations at these limits have similar coordination environments. This is consistent with the experimental results described above. The prdfs are, however, relatively insensitive to subtle changes in coordination number. The most significant differences are seen in the Y–Y structural correlations. In the low-density limit the first peak in the prdf is shifted to higher r with respect to that in the high-density limit and shows a shoulder at low r. Analysis of the cation–cation coordination environments shows that, on average, the Y cations in the low-density limit are coordinated to a greater number of yttriums (*via* oxide bridges) than in the case for the yttrium cations in the high-density limit liquid. Overall, therefore, the yttrium sub-density appears to be more clustered in the low-density limit, and more uniformly distributed in the high-density regime. This interpretation is consistent with the observation that the LDL/LDA phase has lower configurational entropy than the HDL/HDA polyamorph.

5. Conclusion

The diffraction data and the results of simulations confirm the results of our previous work and show unequivocally that the HDL–LDL transition in supercooled Y_2O_3–Al_2O_3 liquids does not involve a change in liquid short-range order (i.e. a change in coordination number). The main structural differences between the high- and low-density phases reflect the way that the different polyhedral structural units are clustered, both the simulation and diffraction studies indicating a shift to higher values of radial distance for the Y–Y correlation. Such subtle changes are consistent with more recent versions of the two-state model in which the two 'crystal-like' species are replaced by the broken and unbroken bonds in a quasi-crystalline lattice [24–26]. In these recent models, the non-ideal interaction parameter (W) of the original Rapoport model [13] is viewed as a measure of cooperativity (clustering) of the excited and non-excited parts of this bond lattice. The properties of the Y_2O_3–Al_2O_3 system resulting in the HDL–LDL transition are simply that the high-temperature liquids in this system are fragile and cooperative.

In conclusion then, it now appears that density- or entropy-driven liquid–liquid phase transitions occurring at constant composition are not only possible, but they may be a quite general aspect of liquid behaviour in many types of system. The behaviour has now been observed or proposed to occur in many elements (S, Se, Te, I, P, C, Si, Ge, Eu, Ba, Cs, ...) and simple systems (H_2O, SiO_2, GeO_2, GeS_2, $GeSe_2$, $AlCl_3$, ...), and in more complex liquids (e.g., Y_2O_3–Al_2O_3 and triphenyl phosphite). These systems represent a wide range of bonding types, packing schemes and chemistry, which leads to our belief in the generality of the phenomenon. In at least some of these systems, the behaviour observed to date is likely to constitute large changes in physical properties in the one-phase regime (i.e., above the critical point), rather than associated with a true liquid–liquid phase transition, or occurs in the non-ergodic glassy regime; however, the existence of such large property changes points to the existence of a density-driven transition at some lower temperature, that may be experimentally inaccessible with current techniques. In several systems studied to date (e.g., S, SiO_2 and Si), the evidence points to the possible existence of multiple L–L transitions occurring in the stable or supercooled liquid phase [10, 11, 15]: it is readily envisaged that the phase diagram of a pure substance may contain a series of polyamorphic transitions as the density is decreased, and that the transition that occurs at lowest density is simply the liquid–gas transformation [15]. The reason why such density-driven transitions have not been more widely recognized is

because they are most likely to occur below the liquidus, in the metastable supercooled liquid regime [10]. This is a consequence of the fact that the thermodynamic energy that drives the transition is generally smaller than the enthalpy of fusion: the result is that the L–L critical temperature lies below the melting point. The other reason is that, in order to observe and characterize a density-driven transition, it is necessary to explore the liquid behaviour over a wide pressure–temperature range. The techniques for this type of study are only now becoming generally available. Now that such techniques exist, the first example of a density-driven HDA–LDA transition has been observed *above* the liquidus, in liquid phosphorus at high pressure [39], even though it might occur between the HDA liquid and the LDA phase in its supercritical fluid state [40].

The existence of such L–L phase transitions driven by density (pressure) and entropy (temperature) differences between the two liquid phases constitutes a new field for exploration in the physical chemistry of the liquid state. For each system in which the phenomenon is described, a major challenge will be understanding the differences in liquid structural configurations that distinguish the two phases, and the factors responsible for the energetic barrier between the two 'landscapes' [55]. It will be necessary to explore the occurrence of multiple L–L transitions within given pure systems, and the variation of the critical temperature as a function of the nature of the density-driven transition. It will also be essential to explore the evolution of unmixing as the onset of 'normal' compositionally driven (chemical potential) transitions is encountered in multicomponent liquid systems [56].

Acknowledgments

Our work on polyamorphism has been supported by the US National Science Foundation, University College London, the Royal Institution and the Wolfson Foundation. Neutron experiments were performed at both the Intense Pulsed Neutron Source (IPNS) at Argonne National Laboratory and at the ISIS pulsed neutron and muon source, Rutherford Appleton Laboratory. High-energy x-ray diffraction studies were performed at the Advanced Photon Source, US Department of Energy, Basic Energy Sciences. PFM is a Wolfson–Royal Society Research Merit Award scholar. MW thanks the Royal Society for a Research Fellowship.

References

[1] Aasland S and McMillan P F 1994 *Nature* **369** 633
[2] Wilding M C and McMillan P F 2001 *J. Non-Cryst. Solids* **293–295** 357
[3] McMillan P F, Ho C T, Aasland S and Weber J K R 1997 *MRS Symp.* **455** 377
[4] Wilding M C and McMillan P F 2002 *NATO Adv. Res. Workshop on New Transformations in Disordered Substances* ed H E Stanley and V Brazhkin (Dordrecht: Kluwer)
[5] Yeganeh-Haeri A, Ho C T, Weber J K R, Diefenbacher J and McMillan P F 1998 *J. Non-Cryst. Solids* **241** 200
[6] Wilding M C, McMillan P F and Navrotsky A 2002 *Physica* A **314** 379
[7] Wilding M C, McMillan P F and Navrotsky A 2002 *J. Phys. Chem. Glasses* **43** 306
[8] Wilding M C, Benmore C J and McMillan P F 2001 *J. Non-Cryst. Solids* **297** 143
[9] Wolf G H, Wang S, Herbst C A, Durben D J, Oliver W F, Kang Z C and Halvorson K 1992 *High-Pressure Research: Application to Earth and Planetary Sciences* ed Y Syono and M H Manghnani (Washington, DC: Am. Geophys. Union) pp 503–17
[10] Poole P H, Grande T, Angell C A and McMillan P F 1997 *Science* **275** 322
[11] Brazhkin V V, Popova S V and Voloshin R N 1997 *High Pressure Res.* **15** 267
[12] Mishima O and Stanley H E 1998 *Nature* **396** 329
[13] Angell C A, Moynihan C T and Yarger J T 2000 *J. Non-Cryst. Solids* **274** 319
[14] Brazhkin V, Buldyrev S V, Ryzhov V N and Stanley H E (ed) 2002 *NATO Adv. Res. Workshop on New Transformations in Disordered Substances* (Dordrecht: Kluwer)

[15] McMillan P F 2002 High pressure phenomena *Proc. Int. School of Physics 'Enrico Fermi',* Course CXLVII, ed R J Hemley, G L Chiarotti, M Bernasconi and L Ulivi (Amsterdam: IOS Press) pp 511–43
[16] Ponyatovsky E G and Barkalov O I 1992 *Mater. Sci. Rep.* **8** 147
[17] Smith K H, Shero E, Chizmeshya A and Wolf G H 1995 *J. Chem. Phys.* **102** 6851
[18] Bridgman P W and Simon J 1953 *J. Appl. Phys.* **24** 405
[19] Williams Q, Hemley R J, Kruger M B and Jeanloz R 1993 *J. Geophys. Res.* **98** 22157
[20] Itié J-P, Polian A, Calas G, Petiau J, Fontaine A and Tolentino H 1989 *Phys. Rev. Lett.* **63** 398
[21] Wolf G H and McMillan P F 1995 *Structure, Dynamics and Properties of Silicate Melts* (*Rev. Mineral.* vol 32) ed J F Stebbins, P F McMillan and D B Dingwell (Washington, DC: Mineralogical Society of America) pp 505–61
[22] Shimomura O, Minomura S, Sakai N, Asaumi K, Tamura K, Fukushima J and Endo H 1974 *Phil. Mag.* **29** 547
[23] Imai M, Mitamura T, Yaoita K and Tsuji K 1996 *High Pressure Res.* **15** 167
[24] Deb S K, Wilding M C, Somayazulu M and McMillan P F 2001 *Nature* **414** 528
[25] Liu L-G and Bassett W A 1986 *Elements, Oxides, Silicates: High-Pressure Phases with Implications for the Earth's Interior* (New York: Oxford University Press)
[26] Young D A *Phase Diagrams of the Elements* (Berkeley: University of California Press)
[27] Tonkov E Y 1992 *High Pressure Phase Transformations* vol 1–3 (Philadelphia, PA: Gordon and Breach)
[28] Hemley R J, Prewitt C T and Kingma K J 1994 *Silica: Physical Behavior, Geochemistry, and Materials Applications* ed P J Heaney, C T Prewitt and G V Gibbs (Washington, DC: Mineralogical Society of America) p 41
[29] Rapoport E 1967 *J. Chem. Phys.* **46** 2891
[30] Rapoport E 1968 *J. Chem. Phys.* **48** 1433
[31] Guggenheim E A 1933 *Modern Thermodynamics by the Methods of Willard Gibbs* (London: Methuen)
[32] Angell C A, Borick S A and Grabow M 1999 *J. Non-Cryst. Solids* **205–207** 463
[33] Di Cicco A, Filipponi A, Itie J-P and Polian A 1996 *Phys. Rev.* B **54** 9086
[34] Di Cicco A *et al* 2003 in preparation
[35] Wilson M and McMillan P F 2003 *Phys. Rev. Lett.* **90** 135703
[36] Hill T L 1994 *Thermodynamics of Small Systems* (New York: Dover)
[37] Chamberlin R V 2002 *Liquid Dynamics. Experiment, Simulation and Theory* (*ACS Symp. Series* vol 820) (Washington, DC: American Chemical Society) p 228
[38] Hill T L and Chamberlin R V 1998 *Proc. Natl Acad. Sci. USA* **95** 12779
[39] Katayama Y, Mizutani T, Utsumi W, Shimomura O, Yamakata M and Funakohi K-I 2000 *Nature* **403** 170
[40] Monaco G, Falconi S, Crichton W A and Mezouar M 2003 *Phys. Rev. Lett.* at press
[41] Coutures J, Rifflet J C, Billard D and Coutures J-P 1987 *Eur. Space Agency Spec. Rep.* **256** 427
[42] Le Floch S, Rifflet J C, Coutures J, Gervais M and Coutures J-P 1993 *Mater. Sci. Eng.* A **173** 185
[43] Gervais M, Le Floch S, Rifflet J C, Coutures J and Coutures J-P 1992 *J. Am. Ceram. Soc.* **75** 3166
[44] Weber J K R, Felton J J, Cho B and Nordine P C 1998 *Nature* **393** 769
[45] Florian P, Gervais M, Douy A, Massiot D and Coutures J-P 2001 *J. Phys. Chem.* B **105** 379
[46] Cockayne B 1985 *J. Less-Common Met.* **114** 199
[47] Cockayne B and Lent B 1979 *J. Cryst. Growth* **46** 371
[48] Caslavsky J L and Viechnicki D J 1980 *J. Mater. Sci.* **15** 1709
[49] McMillan P F, Diefenbacher J T, Ho C-T and Wilding M C 2003 *J. Non-Cryst. Solids* in revision
[50] Wilding M C, Nieman R and McMillan P F 2003 in preparation
[51] Madden P A and Wilson M 1996 *Chem. Soc. Rev.* **25** 339
[52] Domene C, Fowler P W, Madden P A and Wilson M 2002 *Mol. Phys.* **100** 3847
[53] Nosé S 1984 *J. Chem. Phys.* **81** 511
Hoover W G 1985 *Phys. Rev.* A **31** 1695
[54] Martyna G J, Tobias D J and Klein M L 1994 *J. Chem. Phys.* **101** 5
[55] Angell C A 1995 *Science* **267** 1924
[56] Moynihan C T 1997 *Mater. Res. Symp. Proc.* **455** 411